The Vertical Structure of Tropical Convection and Its Impact on the Budgets of Water Vapor and Ozone

IAN FOLKINS AND RANDALL V. MARTIN

Department of Physics and Atmospheric Science, Dalhousie University, Halifax, Nova Scotia, Canada

(Manuscript received 12 February 2004, in final form 8 September 2004)

ABSTRACT

Convective clouds in the Tropics that penetrate the boundary layer inversion preferentially detrain into a shallow outflow layer (2–5 km) or a deep outflow layer (10–17 km). The properties of these layers are diagnosed from a one-dimensional model of the Tropics constrained by observed mean temperature and water vapor profiles. The mass flux divergence of the shallow cumuli (2–5 km) is balanced by a mass flux convergence of evaporatively forced descent (downdrafts), while the mass flux divergence of deep cumulonimbus clouds (10–17 km) is balanced by a mass flux convergence of clear-sky radiative descent. The pseudoadiabatic temperature stratification of the midtroposphere (5–10 km) suppresses cloud outflow in this interval. The detrainment profile in the deep outflow layer is shifted downward by about 1.5 km from the profile one would anticipate based on undilute pseudoadiabatic ascent of air from the boundary layer. The main source of water vapor to most of the tropical troposphere is evaporative moistening. Below 12 km, evaporatively forced descent plays an important role in the vertical mass flux budget of the Tropics. This gives rise to a coupling between the water vapor and mass flux budgets, which, between 5 and 10 km, provides a constraint on the variation of relative humidity with height. Between 12 and 15 km, the observed relative humidity profile can be reproduced by assuming a simple first-order balance between detrainment moistening and subsidence drying. The mean ozone profile of the Tropics can be reproduced using a simple one-dimensional model constrained by the cloud mass flux divergence profile of the diagnostic model.

1. Introduction

It is becoming increasing clear that convective clouds that penetrate the tropical boundary layer inversion fall into two broad categories (Johnson et al. 1996; Zhang and McGauley 2004). Shallow cumuli (e.g., cumulus congestus) are most abundant below the melting level (~5 km), but can detrain as high as 8 km (May and Rajopadhaya 1999; Trenberth et al. 2004). They are responsible for about 28% of the convective rainfall over the western Pacific warm pool (Johnson et al. 1999). Most of the rainfall in the Tropics comes from deep cumulonimbus clouds that detrain between 10 and 17 km, and give rise to the deep, vertically overturning portion of the Hadley circulation.

On the local scale, it is likely that several factors play a role in determining whether or not an individual cumulus cloud develops into a cumulonimbus cloud. These factors include the existence of low-level wind shear (LeMone et al. 1998), the humidity of the lower troposphere (Tompkins 2001; Redelsberger et al. 2002), low-level convergence, and, possibly, the presence of sufficient air in the boundary layer with positive convective available potential energy (CAPE). This paper applies a large-scale thermodynamic perspective to understanding why tropical convective clouds spontaneously segregate into two discrete distributions. It uses a one-dimensional model of the tropical atmosphere to diagnose the strengths of the shallow and deep circulations from the tropical mean budgets of water vapor and dry static energy.

Cloud-mass divergence profiles in the Tropics are usually diagnosed from arrays of vertical profiles of wind, temperature, and humidity surrounding deep convective regions (e.g., Betts 1973; Yanai et al. 1973), and/or radar measurements (Mapes 1995). This approach gives the net mass divergence profile arising from the residual of all diabatic processes inside the domain, including precipitation, cloud radiative heating, evaporative cooling, and turbulent heat transport. Although shallow cumuli can occur in association with deep convection, it is more accurate to think of shallow cumuli as contributing to a steady background condensational heating of the lower troposphere, somewhat analogous to radiative cooling (Mapes 2000). The diabatic mass divergence profiles from arrays surrounding deep convective regions will therefore not include a

Corresponding author address: Dr. Ian Folkins, Dept. of Physics and Atmospheric Science, Dalhousie University, Halifax, NS B3H 3J5, Canada.
E-mail: Ian.Folkins@dal.ca

representative component of the mass divergence from shallow cumulus clouds (although the temperatures of deep convective regions in the interior of these arrays will reflect the existence of shallow convection outside the arrays because of gravity wave propagation). To demonstrate the existence of a distinct shallow circulation in a more physically transparent way, it is desirable to adopt a tropical mean approach. In principle, this approach should enable a better comparison of the effects of shallow cumuli and deep cumulonimbus clouds on the background tropical atmosphere.

The layered aspect of tropical convection has a strong effect on the tropical water vapor budget. The rate at which saturated air detrains from convective clouds is weak between 5 and 10 km. Water vapor is therefore transported to this height interval primarily either through the subsidence of air that had detrained from cumulonimbus clouds at a higher altitude, or from the evaporation of falling ice and water. The specific humidity of the saturated air that detrains from cumulonimbus clouds is extremely low, caused by the extremely cold temperatures of the upper troposphere (>10 km). This air would give rise to relative humidities much lower than the observed value of about 0.3 if directly transported downward to the 5–10 km interval. The main source of water vapor to the interval must therefore be evaporation. The effect of evaporation on the background clear-sky atmosphere depends on the context within which it occurs. Evaporation of cloud droplets and ice crystals occurs when clouds entrain dry air from their environment. This process decreases the buoyancy and detrainment height of clouds, but is otherwise not a direct source of water vapor to the background clear-sky atmosphere. The main mechanism by which evaporation directly moistens the tropical atmosphere is through evaporation associated with precipitation. This occurs, for example, in downdrafts beneath the stratiform anvil. Dry air is drawn toward deep convective systems beneath the stratiform anvil, and this humidified air is subsequently exported to nonactively convecting regions on a lower potential temperature surface. This process will be considered to be a clear-sky process because its net effect is an evaporatively forced descent and moistening of cloud-free air. In the Tropics, the large-scale relative humidity between 5 and 10 km will be mainly determined by how rapidly this precipitation-induced moistening and associated horizontal exchange occurs (Pierrehumbert 1998).

One way to motivate a constraint on the large-scale evaporative moistening of the midtroposphere (5–10 km) by deep convection is to consider the evaporatively driven mass flux within the context of the other sources of vertical motion in the Tropics. These can be considered to be the mean upward mass flux occurring inside clouds, and the radiatively driven downward mass flux occurring in the clear-sky atmosphere. Averaged over the Tropics, these three vertical mass fluxes must approximately sum to zero. The cloud mass flux is weakly dependent on height in the midtroposphere (5–10 km). The vertical variation of the evaporative mass flux is therefore forced to roughly offset the vertical variation of the radiative mass flux, which is itself strongly constrained by the moist pseudoadiabatic temperature structure of the midtroposphere. These considerations put restrictions on the shape of the evaporative moistening profile in the midtroposphere.

2. One-dimensional diagnostic model

Here we describe the tropical mean model of the tropical atmosphere and its assumptions. The model partitions the Tropics into cloudy and clear-sky domains. The cloudy portion of the Tropics is assumed to interact with the clear-sky portion only via a convective detrainment rate d of saturated air, and by the production of condensate, which falls into the clear sky portion of the domain and gives rise to a rate of precipitation-induced evaporative moistening e [kg(H_2O) kg^{-1}(dry air) s^{-1}]. The cloudy portion of the domain is not explicitly modeled. The values of d and e are instead inferred from their effects on the clear-sky atmosphere using the following conservation equations for dry static energy h_d and water vapor mixing ratio r in the clear-sky portion of the tropical atmosphere:

$$(\omega_r + \omega_e)\frac{\partial h_d}{\partial p} = c_p Q_r - L_v e, \tag{1}$$

$$(\omega_r + \omega_e)\frac{\partial r}{\partial p} = e + d(r_s - r). \tag{2}$$

All variables refer to averages over the clear-sky portion of the tropical atmosphere (20°S–20°N). Here, ω_r and ω_e are the mass fluxes associated with radiative cooling and precipitation-induced evaporative cooling, p is pressure, c_p is the specific heat, Q_r is the radiative cooling rate, L_v is the heat of vaporization, and r_s is the saturated water vapor mixing ratio corresponding to the mean tropical temperature. In (1), it is assumed that the vertical advection of dry static energy due to radiative and evaporative descent is balanced by radiative and evaporative cooling. In (2), it is assumed that the vertical advection of the water vapor mixing ratio (subsidence drying) is balanced by evaporative and detrainment moistening.

It can be shown that (1) and (2) follow from more comprehensive closures of the tropical dry static energy and moisture budgets (e.g., Yanai et al. 1973), after restricting attention to the clear-sky portion of the tropical domain and employing several additional approximations. These approximations include the assumption that h_d and r are independent of time and space, that the horizontal advection of h_d and r in and out of the Tropics (here, 20°S–20°N) can be neglected, and that the air detraining from the cloudy portions of

the domain is saturated with h_d (and temperature) equal to the tropical mean. We assume that the tropical mean vertical gradients of h_d and r are the same for both ω_r and ω_e. This is not strictly true, of course, since evaporative cooling occurs in close proximity to deep convection, which can significantly alter both $\partial h_d/\partial p$ and $\partial r/\partial p$ and from their mean values.

Radiative heating rates inside clouds can be substantially different from those in the clear-sky atmosphere (Ackerman et al. 1998), and these differences can have a dramatic effect on tropical convection (e.g., Randall et al. 1989). Although scattering from clouds can also affect radiative heating rates in clear-sky regions, radiative heating rates were calculated (Fu and Liou 1992) without taking this effect into account. Radiative heating that occurs inside clouds is considered to be a diabatic forcing that contributes to ω_c.

In deriving (1) and (2), it was assumed that the fractional area f occupied by cloud at each height was small. Cirrus, cirrostratus, cumulus, and deep convective clouds cover 15.6%, 5.5%, 12.3%, and 2.7% of the tropical area, respectively (Rossow and Schiffer 1999). With the exception of deep convective clouds, the limited vertical extent of most clouds would yield an f, which is probably less than 0.1 at most heights (with the possible exception of the upper tropical troposphere). The $f = 0$ assumption would introduce errors of a similar magnitude. It is also difficult to explicitly account for a nonzero cloudy fractional area in (1) and (2) because the height dependence of f is not well characterized.

Perhaps the most important approximation made in deriving (1) and (2) is that no provision has been made for the entrainment of clear-sky air into the cloudy portion of the domain. It is clear that, in the Tropics, vertical velocities and buoyancies in convective updrafts are smaller than one would anticipate from undilute ascent (e.g., Jorgensen and LeMone 1989; Lucas et al. 1994). The absence of an entrainment parameterization could therefore make the results less realistic. The results obtained are, however, not specific to particular assumptions about how convective updrafts mix with their environment, assumptions that are still quite speculative.

In deriving (1), it was assumed that the only sources of vertical motion in the clear-sky portion of the domain were those associated with radiative and evaporative cooling (i.e., $\omega = \omega_e + \omega_r$). This neglects, for example, the dynamically induced clear-sky subsidence that occurs in response to the net upward fluxes in clouds. It is not possible to include adiabatic vertical velocities in a one-dimensional model in which the heights of dry static energy surfaces are kept fixed. The effects of dynamically induced adiabatic warming are, however, included in the model because the model is constrained by observed temperature profiles. Dynamically induced descent warms the tropical troposphere, increases radiative cooling rates, and increases ω_r.

The rate of precipitation-induced evaporative moistening e obtained from (1) and (2) refers only to that component of the total evaporation that contributes to an increase in the observed tropical mean r. Although the entrainment of dry air into clouds can result in evaporation, the main effect of this process is to lower the final detrainment profile of the cloud. Evaporation of precipitation can also occur within very vigorous convective downdrafts that directly inject midtropospheric air into the boundary layer. The evaporation occurring in this type of downdraft does not play a role in directly increasing the clear-sky water vapor mixing ratio, and therefore does not contribute to e.

The set of Eqs. (1) and (2) contain eight potentially independent variables. However, four of these variables can be constrained by observations (h_d, Q_r, r, and r_s), while ω_r and Q_r, and ω_e and e are directly coupled. Equations (1) and (2) therefore constitute a solvable system of equations in two unknowns (e and d).

Tropical mean profiles of h_d and r were obtained from radiosonde observations. To get a reasonable coverage between 20°S and 20°N, we used 12 radiosonde stations from the Stratospheric Processes and their Role in Climate (SPARC) high-resolution data archive, and 12 radiosonde stations from the Southern Hemisphere Additional Ozonesondes (SHADOZ) archive (Thompson et al. 2003). Figure 1 shows the locations of these twenty-four radiosonde sites. Seasonal means were generated within 10° latitude bands. Tropical means were generated by averaging over all latitudes and seasons. We used radiosonde data from the SPARC archive for the years 1999–2001. Radiosondes were launched up to twice daily, generating up to 1000 profiles at each location. At most of the SHADOZ sites, the radiosonde data used extended from 1998 to 2001, with typically at least 100 profiles available.

3. The tropical mass budget

The radiative and evaporative mass fluxes can be expressed in terms of their associated diabatic forcings as

$$\omega_r = \frac{Q_r}{\sigma}, \tag{3}$$

$$\omega_e = -\frac{L_v e}{c_p \sigma}, \tag{4}$$

where the static stability σ has various equivalent forms, including (e.g., Holton 1992)

$$\sigma = \frac{(\Gamma_d - \Gamma)}{\rho g} = -\frac{T}{\theta}\frac{\partial \theta}{\partial p} = \frac{\partial}{\partial p}\left(\frac{h_d}{c_p}\right). \tag{5}$$

Here, Γ is the lapse rate ($= -dT/dz$), Γ_d is the dry adiabatic lapse rate, and $h_d = c_p T + gz$ is the dry static energy.

Figure 2 shows annual mean profiles of σ at the five SPARC radiosonde stations in the western tropical Pa-

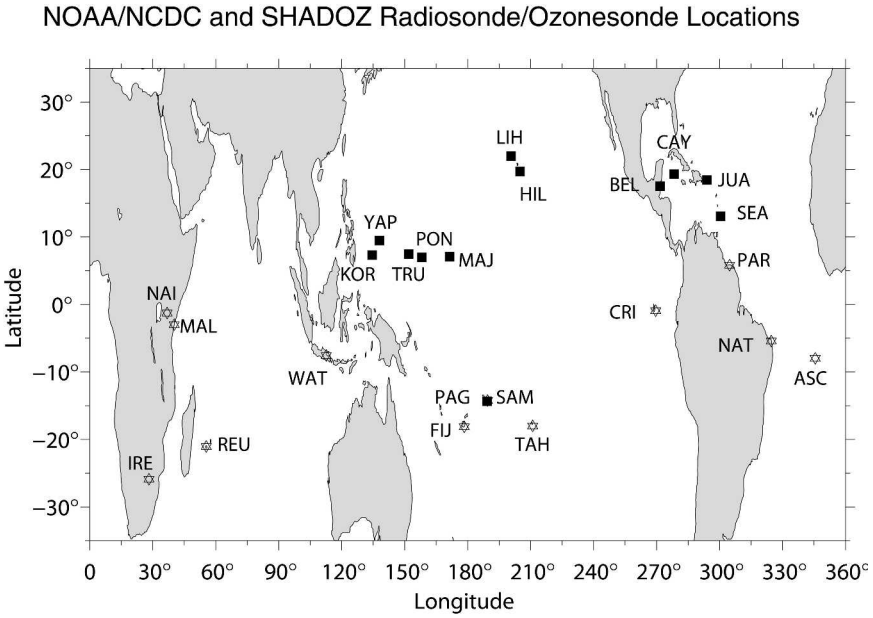

FIG. 1. Locations of the tropical NOAA/NCDC radiosondes used in this paper. Each location has been identified by a three letter code: BEL (Belize), CAY (Grand Cayman), HIL (Hilo, Hawaii), JUA (San Juan/Isla Verde, USA), KOR (Koror/Palau Island), LIH (Lihue/Kauai, Hawaii), MAJ (Majuro/Marshall Islands), PAG (Pago Pago International Airport, Samoa), PON (Ponape Island), SEA (Seawell, Barbados), TRU (Truk International Airport/Moen Island), and YAP (Yap Island). Shown in stars are the locations of the SHADOZ radiosonde/ozonesonde sites: NAI (Nairobi), MAL (Malindi), WAT (Watukosek), IRE (Irene), REU (La Reunion), PAG (American Samoa), FIJ (Fiji), TAH (Tahiti), CRI (San Cristobal), PAR (Paramaribo), NAT (Natal), and ASC (Ascension Island).

cific. The dashed curve is the σ of a moist pseudoadiabat, starting at the surface with a pseudoequivalent potential temperature (θ_{ep}) equal to 350 K. (In pseudoadiabatic ascent, condensate is removed upon formation. In reversible adiabatic ascent, condensate is retained by the air parcel.) The magnitude of the observed σ has a maximum at the top of the convective boundary layer (2 km). It deviates significantly from the pseudoadiabatic σ between the top of the convective boundary layer and the melting level. We will refer to this interval as the shallow outflow layer. The observed σ is in good agreement with the σ of the water pseudoadiabat between the melting level and 10 km. This interval will be referred to as the pseudoadiabatic layer. The interval between 10 km and the top of upper limit of deep convective outflow will be referred to as the deep outflow layer.

The dotted curve in Fig. 2 shows the ice pseudoadiabat, in which water vapor condenses to ice rather than water above the melting level. Ice nucleation is expected to occur within marine tropical deep convective updrafts soon after updrafts cross the melting level (e.g., Zipser 2003). It is therefore somewhat surprising that the observed σ matches the water pseudoadiabat much more closely than the ice pseudoadiabat.

Figure 3 shows the profiles of Q_r and Q_e generated by the one-dimensional model ($Q_e = -L_v e/c_p$). Above 12 km, saturated water vapor pressures are sufficiently small that evaporative cooling is unable to compete with radiative cooling. This decouples the water vapor and dry static energy budgets. The rate of precipitation-induced evaporative cooling is larger at higher temperatures of the lower troposphere and, in particular, is larger than radiative cooling in most of the shallow outflow layer (2–5 km).

The tropical mean clear-sky radiative mass flux generated by the model is shown in Fig. 4. The peak in ω_r at 11 km is due to the weakness of the static stability in much of the upper troposphere (10–13 km; Mapes 2001).

In the model, the downward mass fluxes from clear-sky radiative cooling and precipitation-induced evaporative cooling are offset by an upward mass flux occurring inside clouds. The sum of all three vertical mass fluxes should therefore equal zero. (This assumes that the net exchange of mass between the Tropics and midlatitudes can be assumed small, the validity of which will be addressed in a later section.) Let f refer to the fractional area of the Tropics occupied by clouds at a given height, and let ω_c' refer to the average mass flux occurring in the cloudy portion of the domain. One can then write

$$(1 - f)\omega_r + (1 - f)\omega_e + f\omega_c' = 0. \quad (6)$$

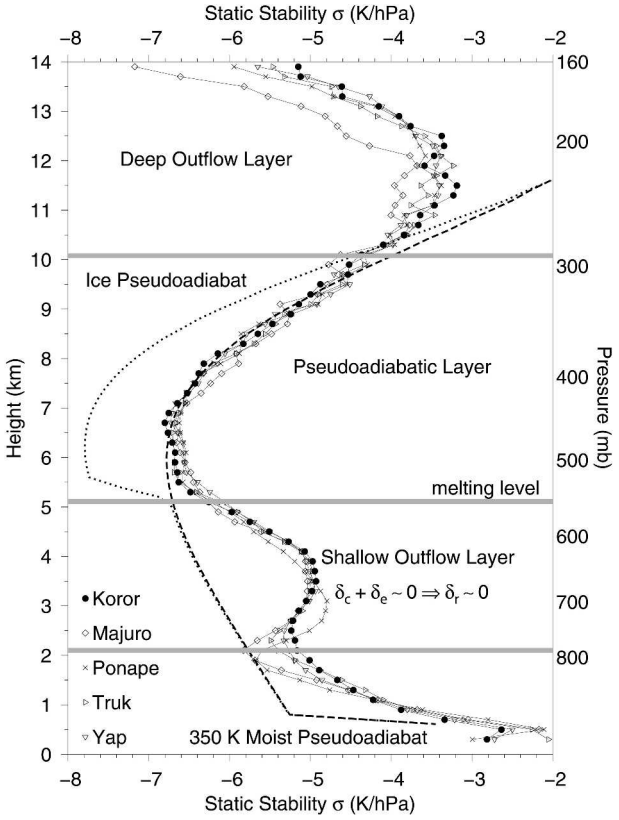

FIG. 2. Annual mean profiles of static stability σ at five radiosonde locations in the western tropical Pacific. The thick dashed line represents the static stability of a 350-K moist pseudoadiabat. The dotted line is the static stability of a 350-K moist pseudoadiabat in which water vapor is assumed to condense to ice above the melting level. The pseudoadiabatic layer has been defined as the interval between 5 and 10 km, where the observed static stability most closely approximates a moist pseudoadiabat.

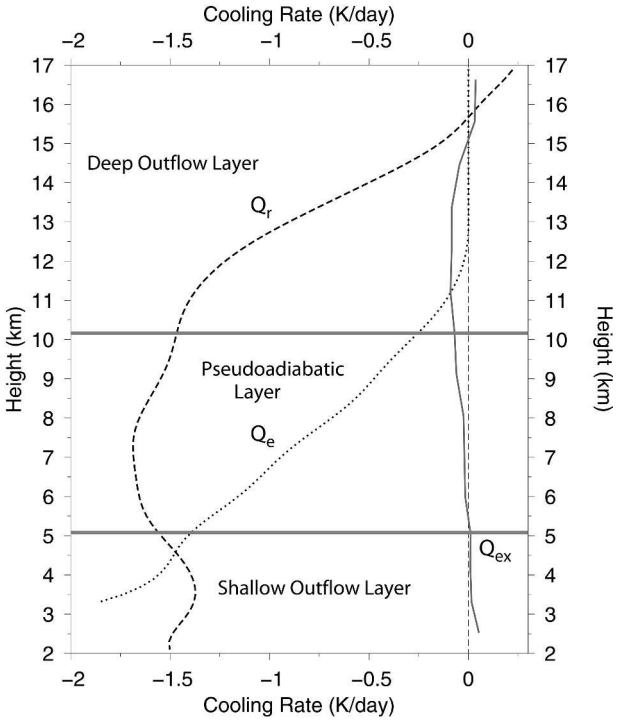

FIG. 3. Here, Q_r and Q_e refer to the tropical mean (20°S–20°N) clear-sky radiative and evaporative cooling rates predicted by the one-dimensional diagnostic model, and Q_{ex} refers to the effective tropical mean cooling associated with eddy transport of dry static energy to the extratropics.

It is convenient to define $\omega_c = \omega_c' f/(1 - f)$, so that ω_c represents the cloud mass flux averaged over the clear-sky portion of the Tropics. This gives

$$\omega_r + \omega_e + \omega_c = 0. \tag{7}$$

Figure 4 shows the vertical variation of the cloud mass flux ω_c obtained from the solutions for ω_r and ω_e. Between 6 and 10 km, the vertical variation of ω_e offsets the vertical variation of ω_r, so that the cloud-mass flux ω_c is weakly dependent on height.

The mass flux divergence associated with clear-sky radiative cooling is defined as

$$\delta_r = -\frac{\partial \omega_r}{\partial p}. \tag{8}$$

The mass flux divergences δ_c and δ_e associated with the cloud heating and precipitation-induced evaporative cooling can be defined in an analogous way. Using (7), one can show that the mass flux divergences associated with the tropical mean clear-sky radiative cooling, precipitation-induced evaporative cooling, and cloud heating, sum to zero,

$$\delta_r + \delta_e + \delta_c = 0. \tag{9}$$

The vertical variation of each of these mass divergences is shown in Fig. 5. Deep cumulonimbus clouds are associated with an enhanced cloud divergence δ_c in the deep outflow layer, while shallow cumuli are associated with enhanced δ_c in the shallow outflow layer.

Figure 5 shows that the mass flux divergence from clouds in the deep outflow layer is balanced mainly by a mass flux convergence from clear-sky radiative cooling. Temperatures are sufficiently cold in most of this layer that $\omega_e \approx 0$. This implies $\delta_r + \delta_c \approx 0$. The mass flux divergence from clouds in the shallow outflow layer is balanced mainly by the evaporative mass flux divergence. Within this layer, the tropical mean static stability σ and clear-sky radiative cooling have a similar dependence on height, so that ω_r is roughly constant and $\delta_r \approx 0$. This implies $\delta_e + \delta_c \approx 0$. The mass flux divergence from clouds is weak within the pseudoadiabatic layer (5–10 km).

Cloud-mass flux divergence profiles diagnosed from measurements are sensitive to the spatial scale of the region under consideration. Divergence profiles diagnosed from arrays of radiosonde measurements in ac-

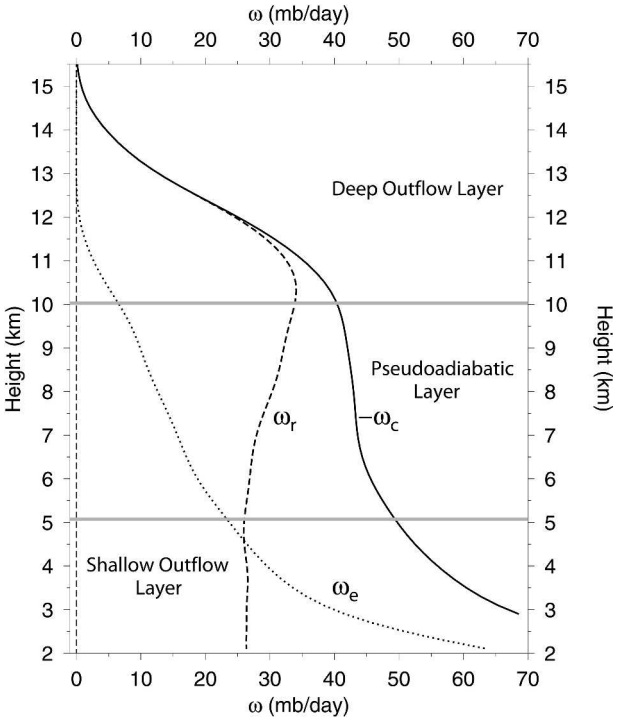

FIG. 4. Tropical mean (20°S–20°N) vertical velocities associated with diabatic processes in clouds (ω_c), clear-sky radiative cooling (ω_r), and clear-sky evaporative cooling (ω_e).

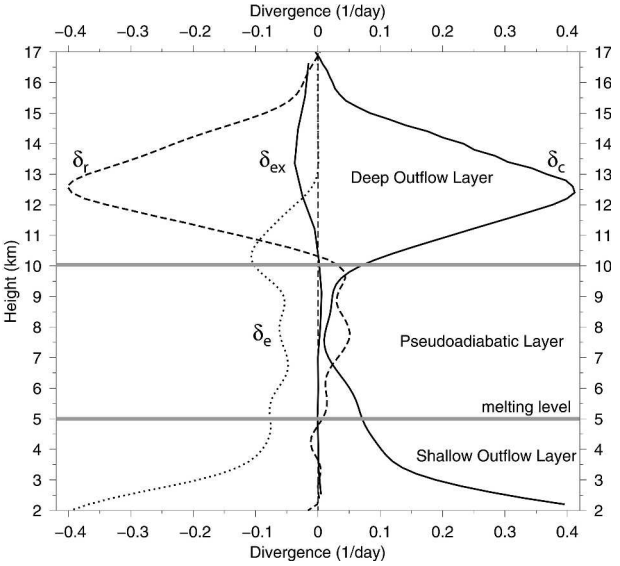

FIG. 5. Tropical mean (20°S–20°N) vertical profiles of cloud-mass divergence δ_c, clear-sky radiative mass divergence δ_r, and evaporative mass divergence δ_e. Here, δ_{ex} refers to the tropical mean divergence associated with transport between the Tropics and extratropics. A positive mass divergence refers to a source of mass to the clear-sky atmosphere while a negative mass divergence refers to a sink of mass from the clear-sky atmosphere.

tively convecting regions are typically bimodal, with a deep convective "hot tower" mass divergence peak in the upper troposphere, reduced mass divergence in the midtroposphere, and enhanced mass divergence in the boundary layer (e.g., Yanai 1973). Divergence profiles obtained using radar measurements in the immediate vicinity of deep convective mesoscale systems tend to be convergent below 400 mb (Mapes and Houze 1993; Mapes 1995). We presume this is mainly because the evaporative mass flux convergence within these systems is not being offset by a larger-scale mass flux divergence from shallow cumuli. The cloud-mass flux divergence profiles of deep convective systems also change shape as the systems evolve from the vigorously convecting stage toward the stratiform anvil stage. Mean divergence profiles from the vigorously convecting stage, during which the relative importance of precipitation-induced evaporative mass fluxes is likely to be reduced, also show near-zero divergence between 5 and 10 km (Fig. 6 of Houze 1997).

Figure 6 gives an overview of the vertical structure of the tropical troposphere, motivated by the cloud-mass flux divergence profile shown in Fig. 5 and the static stability profiles shown in Fig. 2.

4. The tropical water vapor budget

The tropical mean relative humidity profile used by the model is shown in Fig. 7. Below 11 km, the mean profile was obtained by averaging over the 12 SPARC and 12 SHADOZ humidity profiles. Relative humidity measurements from radiosondes are considered to be inaccurate in the upper troposphere, and are not shown above 12 km. Figure 7 also shows a tropical mean relative humidity profile obtained from the Microwave Limb Sounder (MLS; Read et al. 2001). Differences among the datasets underline the importance of obtaining additional water vapor measurements in the upper tropical troposphere.

Figure 8 shows the relative humidity profile generated by setting $e = 0$ in Eqs. (1) and (2). In this case, r can be obtained from

$$\omega_r \frac{\partial r}{\partial p} = d_r(r_s - r), \tag{10}$$

where $d_r = \delta_r = \partial\omega_r/\partial p$. In this profile, detrainment moistening (calculated from the radiative mass divergence) is balanced by subsidence drying (calculated from the radiative mass flux). The $e = 0$ relative humidity profile is very similar to the aircraft climatology between 12 and 15 km, suggesting that the mean water vapor budget in this interval assumes a particularly simple first-order balance (Dessler and Sherwood 2000; Folkins et al. 2002b).

The height dependence of the subsidence drying, evaporative moistening, and detrainment moistening terms in the water vapor budget are shown in Fig. 9. Each term has been normalized by r to give it units of inverse time. For example, the precipitation-induced

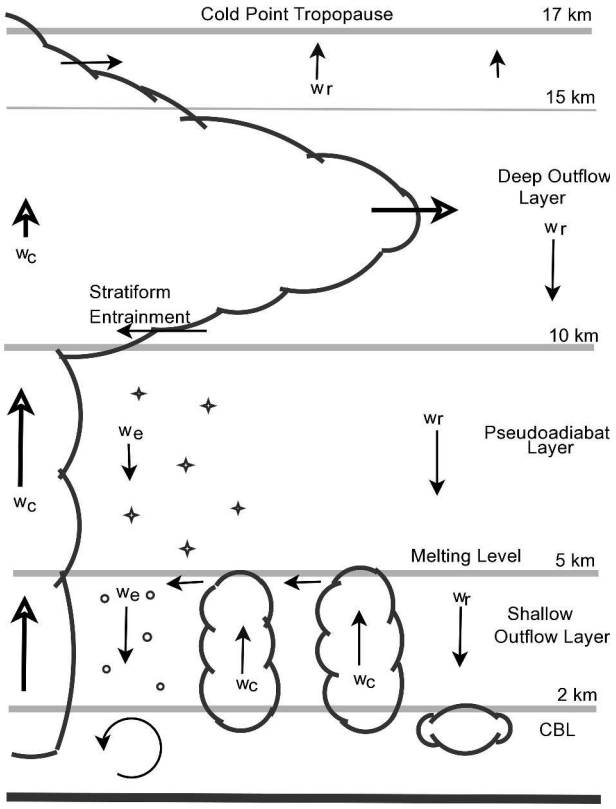

FIG. 6. A representation of the vertical structure of the tropical troposphere. The vertical mass fluxes associated with in-cloud heating, clear-sky evaporative cooling, and clear-sky radiative cooling are labeled ω_c, ω_e, and ω_r, respectively. The level of zero clear-sky radiative cooling occurs near 15 km. Air parcels that detrain above this level have a much higher probability of ascending into the stratosphere than those that do not.

evaporative moistening source (e/r) of 0.5 day^{-1} at 10 km implies that precipitation-induced evaporation supplies a source of water vapor every day equal to half the ambient tropical mean water vapor at that height.

5. Extratropical exchange of mass, dry static energy, and water vapor

In deriving (1), (2), and (9) it was assumed that the exchange of mass, dry static energy, and water vapor between the Tropics (here 20°S–20°N) and the extratropics could be neglected in comparison to other terms in these equations. In this section, we use assimilated meteorological data from the Goddard Earth Observing System (GEOS) of the NASA Data Assimilation Office to estimate the errors introduced by these assumptions. The model has a horizontal resolution of 2° latitude and 2.5° longitude. The dataset has a vertical resolution of approximately 1 km in the troposphere, and was archived every 6 h. An annual average was obtained by averaging over January, April, July, and October of 1997.

Figure 5 shows the mass divergence δ_{ex} associated with mass exchange between the Tropics and extratropics. There is a small convergent flow of mass from the extratropics into the Tropics between 7 and 10 km. (The sign convention is with respect to the cloud-free tropical atmosphere, so that a positive δ_{ex} is a source of mass.) The direction of this net flow changes sign at the base of the deep outflow layer (10 km) and is largest at 13.5 km. Below the level of zero, clear-sky radiative heating (~15.2 km), the divergence of mass from the Tropics δ_{ex} is much smaller than the cloud-mass divergence δ_c, and (9) is a reasonable approximation.

The use of (7) assumes that any upward convective mass flux between 20°S and 20°N is exactly offset by radiative and evaporatively induced descent. To determine the accuracy of this assumption, the mass divergence profile δ_{ex} obtained from the GEOS output was used, together with the assumption $\omega = 0$ at the surface, to compute the vertical variation of the tropical mean mass flux due to the exchange of mass with the extratropics. It reached a maximum upward mass flux of 3 mb day near 10 km. This is much smaller than the tropical mean vertical mass fluxes associated with diabatic

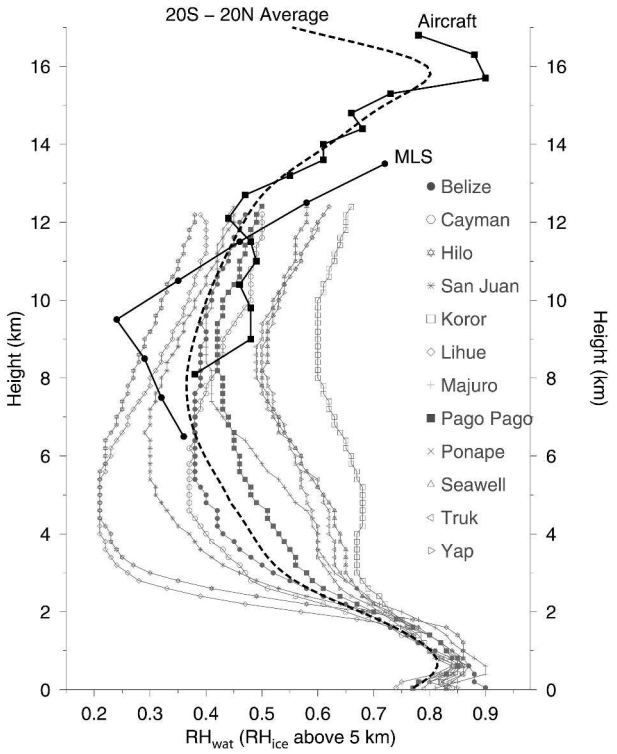

FIG. 7. The dashed curve is the tropical mean relative humidity profile used in the diagnostic model. This mean profile was constrained by radiosonde measurements below 11 km, and by an aircraft climatology (Folkins et al. 2002b) between 12.5 and 15 km. The annual mean relative humidity profiles from the SPARC radiosonde locations are shown in gray. The aircraft climatology is indicated using solid black boxes. The curve indicated using solid circles is a 20°S–20°N relative humidity climatology from the MLS.

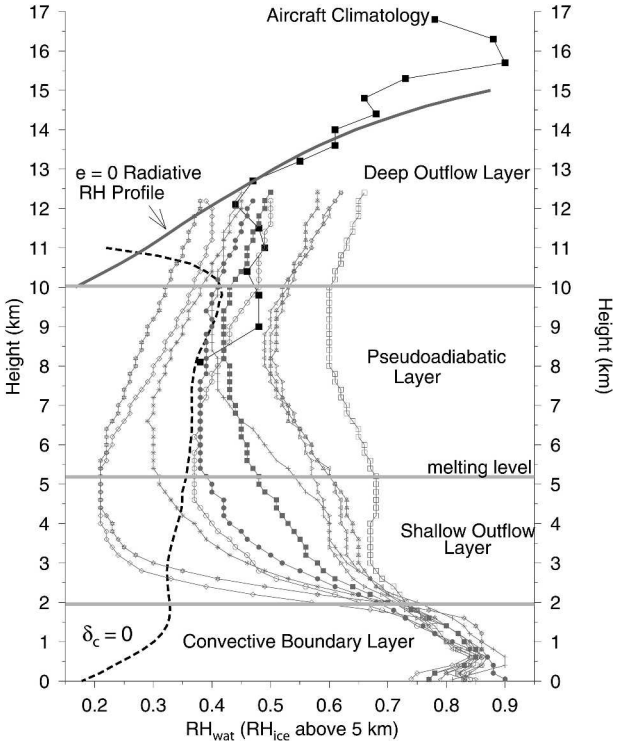

FIG. 8. The dashed curve labeled $\delta_c = 0$ refers to the relative humidity profile generated by assuming that the cloud divergence is zero, so that the precipitation-induced mass flux divergence and the radiative mass flux divergence directly offset one another ($\delta_e + \delta_r = 0$). The relative humidity profile generated from this assumption is in good agreement with an average of the observed profiles between 5 and 10 km. Annual mean relative humidity profiles of the SPARC radiosonde sites are shown in gray. The locations corresponding to each symbol are same as in Fig. 7. The curve with solid boxes is an aircraft climatology (Folkins et al. 2002b). Between 12 and 15 km, it agrees quite well with the $e = 0$ radiative relative humidity profile, shown in gray. The $e = 0$ profile was obtained from (10), which assumes a first-order balance between subsidence drying and detrainment moistening.

processes, and indicates that (7) is a reasonable assumption.

The zonal mean export of dry static energy from the Tropics can be written as a sum of contributions from the mean flow and transport by eddies,

$$\langle h_d \rho v \rangle = \langle h_d \rangle \langle \rho v \rangle + \langle h_d' (\rho v)' \rangle, \tag{11}$$

where $h_d' = h_d - \langle h_d \rangle$, v is the meridional velocity, and ρ is the density. If the diagnostic model were to allow an export of mass from the Tropics by the mean circulation, the associated mean transport of dry static energy would be compensated by the detrainment of dry static energy from clouds. (Dry static energy is assumed to be horizontally homogeneous.) In this case, the most physically relevant way to estimate the effect of transport on the mean tropical dry static energy budget is to compare the eddy sink of dry static energy from the Tropics with radiative and evaporative cooling. An effective heating rate of the Tropics due to eddy exchange of dry static energy was calculated by adding $\langle h_d' (\rho v)' \rangle$ from 20°S and 20°N, and normalizing the sum by the mass of the pressure interval. Figure 3 shows the resulting tropical mean effective heating rate Q_{ex}. On average, eddy transport of dry static energy cools the Tropics between 5 and 15 km, and warms elsewhere. The only height range where it is of comparable importance with radiative cooling is in the immediate vicinity of the level of zero radiative heating (~15 km).

An estimate of the importance of extratropical exchange on the tropical water vapor budget was obtained by calculating $\langle r v \rho \rangle$ from the GEOS model, adding the contributions from both hemispheres, and normalizing the total export of water vapor from each pressure interval by the mass of water vapor in that interval. The importance of this exchange relative to the other terms in the mean tropical water vapor budget is shown in Fig. 9. As expected, this exchange gives rise to a net loss of water vapor from the Tropics. It occurs at an approximate rate of 0.025 day^{-1} at all

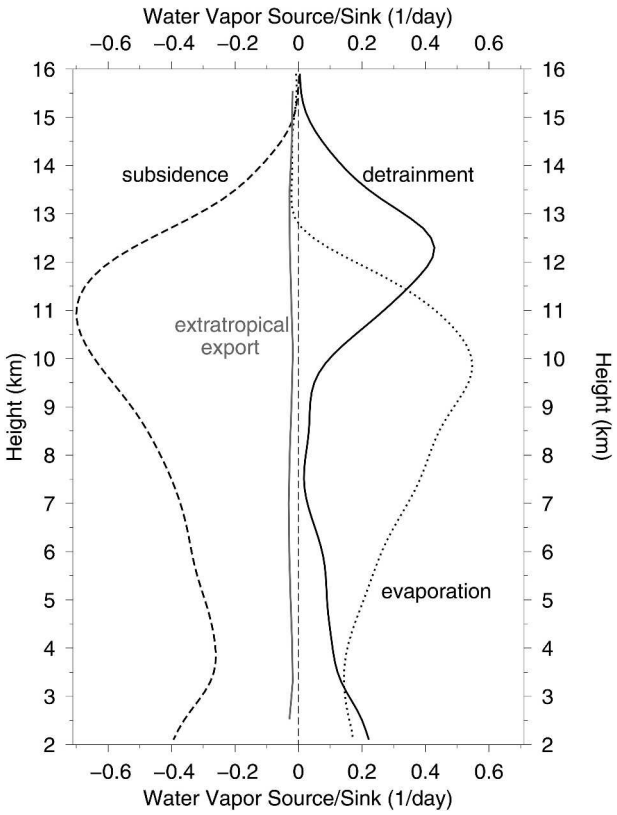

FIG. 9. Tropical mean (20°S–20°N) vertical profiles in terms in the water vapor budget from Eq. (2). The subsidence term is defined as $(1/r)(\omega_r + \omega_e)\delta r/xp$, the evaporative term as e/r, and the detrainment term as $d(r_s - r)/r$, where r refers to the tropical mean water vapor mass mixing ratio at that height. The inverse of each term gives the time scale at which that process removes or produces water vapor at that altitude. The extratropical export term is defined similarly.

heights (i.e., the time scale for the removal of water vapor from the 20°S–20°N latitude interval is approximately 40 days). Below 15 km, this is substantially smaller than the other terms in the water vapor budget.

6. A simple ozone model

The cloud-mass divergence profile shown in Fig. 5 is forced by definition to generate the observed mean relative humidity profile. It can, however, be independently tested by determining whether or not it generates realistic mean profiles of other trace species. Ozone is an important constituent of the atmosphere, both from a radiative point of view, and also because it produces the hydroxy radical OH, the main oxidant of the atmosphere. By analogy with (8), one can write the following budget expression for the conservation of cloud-free ozone mixing ratio O_3:

$$(\omega_r + \omega_e)\frac{\partial O_3}{\partial p} = P + d(O_{3,\text{conv}} - O_3), \qquad (12)$$

where the term on the left-hand side of the equation represents the vertical advection of ozone (arising from both radiatively and evaporatively induced mass fluxes), P is the net chemical production, and $d(O_{3,\text{conv}} - O_3)$ is the convective detrainment tendency ($d = \delta_c$ under our assumptions). Below 15.5 km, the tropical mean P was calculated with the Goddard Earth Observing System-Chemistry (GEOS-CHEM) three-dimensional chemical transport model v4.26 (Martin et al. 2003). Above 15.5 km, it was determined from direct measurements of ozone and its precursors (see Folkins et al. 2002a for details). Here, $O_{3,\text{conv}}$ represents the mean ozone mixing ratio detraining from tropical convective clouds and is the only free parameter in the model. In the absence of entrainment, it would approximately equal the mean mixing ratio of ozone in the convective boundary layer.

The dashed lines in Fig. 10 represent the ozone profiles generated by the model with $O_{3,\text{conv}} = 20$ ppbv and $O_{3,\text{conv}} = 30$ ppbv. Mean ozone mixing ratios below 2 km range from 15 to 30 ppbv. We find that $O_{3,\text{conv}} = 20$ ppbv is more representative of marine convection, while $O_{3,\text{conv}} = 30$ ppbv is more representative of continental convection. Figure 10 also shows the mean ozone profiles at the ten SHADOZ sites within 20 degrees of the equator. Each of the ten profiles has a similar "S shape" which is well reproduced by both model simulations. The broad upper tropospheric minimum in ozone is associated with a maximum in the convective detrainment of low-ozone air from the boundary layer.

Ozone profiles at the four sites associated with continuous or seasonally active deep marine convection (Java, Samoa, Fiji, Tahiti) are in good agreement with the $O_{3,\text{conv}} = 20$ ppbv model profile. Ozone profiles at the four continental locations (Malindi, Nairobi, Natal, Paramaribo), and at the two island locations likely to be strongly influenced by continental convection (Ascension and San Cristobal) tend to be close to, or somewhat larger than, the $O_{3,\text{conv}} = 30$ ppbv model profile.

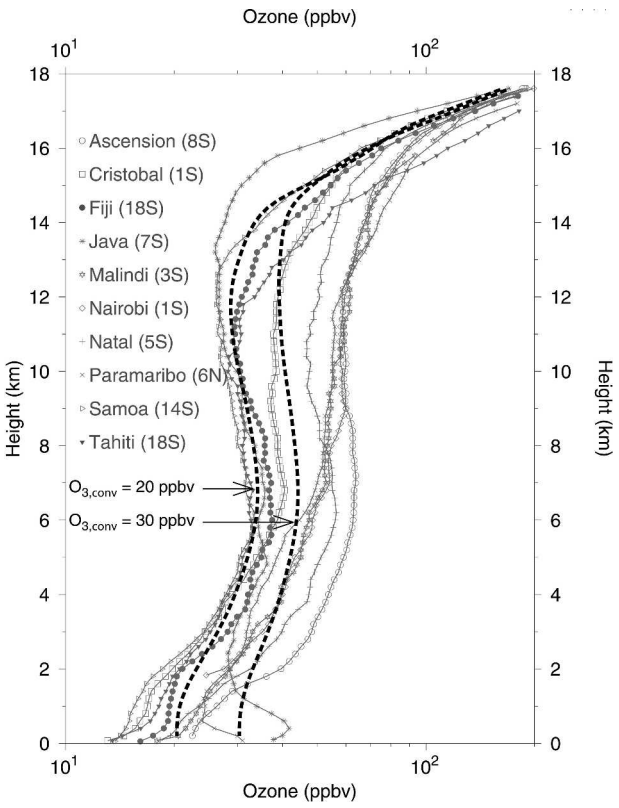

FIG. 10. The profiles shown in gray are mean ozone climatologies at the SHADOZ ozonesonde stations between 20°S and 20°N. The dashed lines refer to ozone profiles generated by (12) with different values of $O_{3,\text{conv}}$, which refers to the mean ozone mixing ratio of air parcels detraining from convective clouds.

7. The undilute ascent model

The level of neutral buoyancy of an air parcel rising from the surface in an updraft occurs at the height where the θ_{ep} of the air parcel becomes equal to the saturated pseudoequivalent potential temperature θ^*_{ep} of the background atmosphere. This assumes that the air parcel experiences undilute ascent and that virtual temperature effects can be ignored. In the upper troposphere, water vapor mixing ratios are sufficiently low that $\theta^*_{ep} \approx \theta$. Figure 11 shows δ_c using θ as a vertical coordinate. The deep outflow mode extends from 340 to 365 K. This roughly corresponds to the range of pseudoequivalent potential temperatures observed in the boundary layer of actively convecting regions. It has therefore been suggested that, to first order, cumulonimbus hot towers directly transport air from the boundary layer into the upper troposphere (Riehl and Simpson 1979). This gives rise to an apparent paradox, however, since the temperatures and vertical velocities

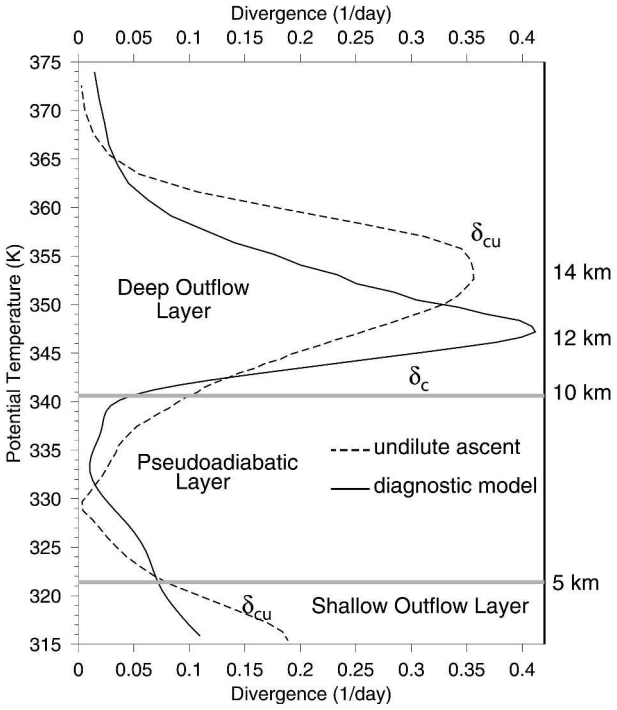

FIG. 11. The solid curve labeled δ_c refers to the convective mass flux divergence determined from the diagnostic model (also shown in Fig. 5). The dashed curve labeled δ_{cu} refers to the mass flux divergence profile determined from (15) using the assumption of undilute ascent.

observed within tropical convective updrafts are almost always less than predicted by undilute parcel theory (Jorgensen and LeMone 1989; Lucas et al. 1994). In this section, we attempt to resolve this paradox by showing that the assumption of undilute ascent generates an upper-tropospheric mass divergence profile (δ_{cu}) that peaks at a higher altitude than the divergence profile obtained from the diagnostic model (δ_c). The amount of entrainment implied by this height offset is roughly consistent with that required to reduce undilute updraft velocities to their observed values.

Figure 12 shows probability distribution functions (PDFs) of θ_{ep} in the boundary layer in various SST ranges. The PDFs have been generated from three years (1999–2001) of temperature, relative humidity, and pressure profiles at the SPARC radiosonde locations shown in Fig. 1. Monthly sea surface temperatures at the SPARC locations were obtained from the Reynolds SST analysis (Reynolds et al. 2002). Air parcels above the 800-mb level did not contribute to the PDFs because such air parcels rarely have positive CAPE and are therefore unlikely to rise into the upper troposphere by undilute ascent (Folkins 2002). The dashed line in Fig. 12 is a tropical mean θ_{ep} PDF, calculated from an area-weighted average of the individual PDFs shown in Fig. 12.

Figure 13 illustrates the procedure by which an observed θ_{ep} PDF was used to generate an undilute cloud-mass divergence profile. Suppose two air parcels are entrained into a convective updraft from the boundary layer, one with θ_{ep} slightly less than 345 K, and one with θ_{ep} slightly greater than 345 K. In the case of undilute pseudoadiabatic ascent, the θ_{ep} of the air parcels will be conserved, and they will travel upward along constant θ_{ep} trajectories as indicated by the vertical lines in Fig. 13. The parcels will be neutrally buoyant at the heights at which their θ_{ep} is equal to the saturated pseudoequivalent potential temperature θ^*_{ep} of the background atmosphere. This occurs first at the level of free convection and then at the level of neutral buoyancy. The tropical mean 20°S–20°N θ^*_{ep} climatology is indicated by the solid line in the upper part of Fig. 13.

If all air parcels in the boundary layer with positive CAPE have equal probability of participating in deep

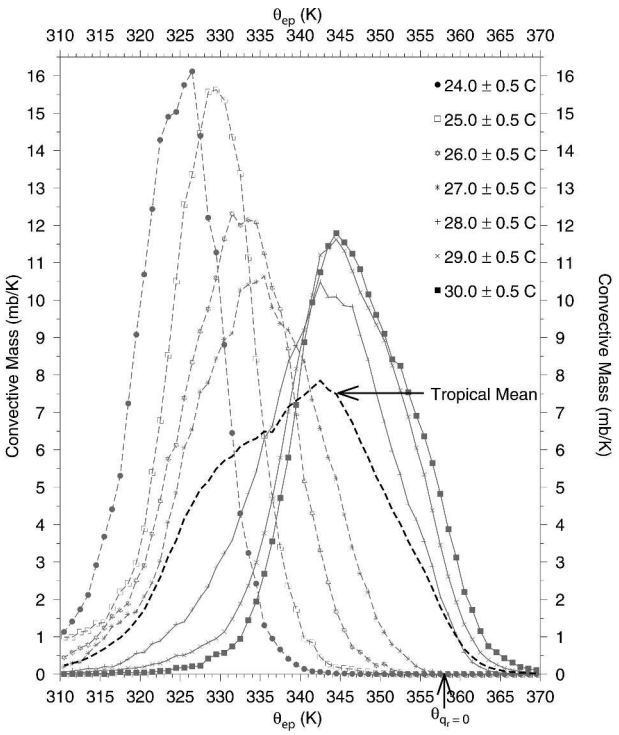

FIG. 12. Each curve is a PDF of θ_{ep} in the boundary layer obtained from radiosonde profiles in a specified SST range. The PDF is obtained by counting over all measurements between the 1010- and 800-mb levels (with all pressure intervals weighted equally). The units are given as mb K^{-1}, so that the integral of each PDF over all θ gives 210 mb. The dashed line is a tropical mean θ_{ep} PDF obtained by averaging over the PDFs in each of the SST ranges. The contribution of each PDF to the tropical mean was weighted by the area occupied by that SST interval (20°S–20°N); $\theta_{qr} = 0$ refers to the mean potential temperature of the level of zero radiative heating. The area of the convective θ_{ep} distribution to the right of $\theta_{qr} = 0$ is a measure of the amount of air in the boundary layer that can detrain above the level of zero radiative heating by undilute ascent. In this case, air parcels with θ_{ep} greater than 357 K have the greatest likelihood of ascending into the stratosphere. The θ_{ep} PDFs become insensitive to increases in the underlying SST for SSTs larger than 28°C.

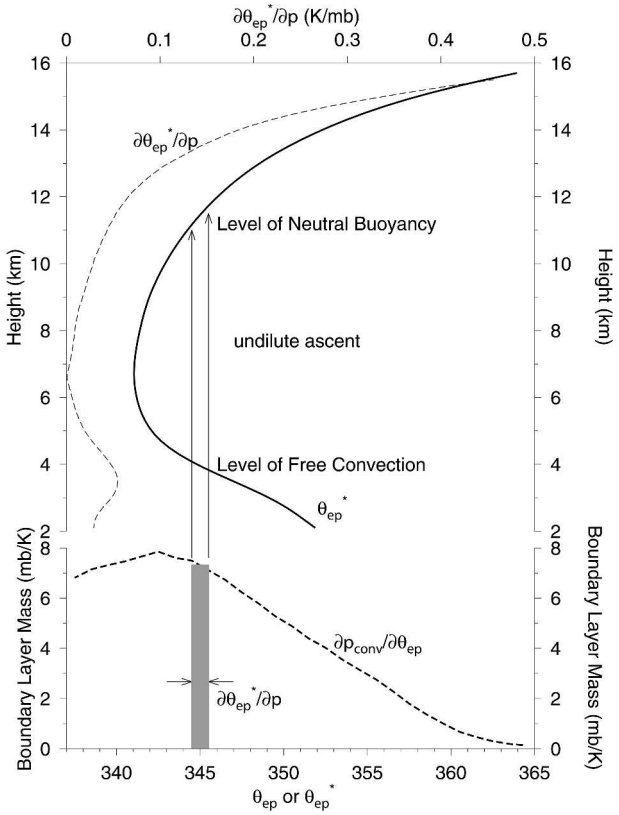

FIG. 13. The dashed curve in the lower panel refers to the tropical mean boundary layer θ_{ep} probability distribution function discussed in the caption to Fig. 12. The solid line in the upper panel is a tropical mean θ_{ep}^* profile. The thin dashed line in the upper panel is a tropical mean $\partial\theta_{ep}^*/\partial p$ profile, and is a measure of the density of available θ_{ep}^* states to which air parcels can detrain. Air parcels undergoing undilute ascent from the boundary layer will rise upward along straight lines, first crossing the level of free convection, and then the level of neutral buoyancy.

convection, the convective outflow δ_{cu} into a pressure interval Δp will be proportional to the $\Delta\theta_{ep}^*$ of this interval, since this gives the amount of available θ_{ep}^* states to which air parcels undergoing undilute pseudoadiabatic ascent from the surface can detrain,

$$\delta_{cu} \propto \Delta\theta_{ep}^* = \frac{\partial\theta_{ep}^*}{\partial p}\Delta p. \tag{13}$$

In Eq. (13), δ_{cu} will also depend on the mass of air in the boundary layer thermodynamically able to detrain into the Δp interval under our assumptions. This is equal to the value of the θ_{ep} PDF at the mean θ_{ep}^* of the Δp interval ($\partial p_{CBL}/\partial\theta_{ep}$), so that

$$\delta_{cu}(\theta_{ep}^*) \propto \frac{\partial p_{CBL}}{\partial\theta_{ep}}\frac{\partial\theta_{ep}^*}{\partial p}\Delta p. \tag{14}$$

Figure 13 shows how (14) can be interpreted graphically. The undilute cloud-mass divergence (δ_{cu}) of a pressure interval is proportional to its projected area under the θ_{ep} PDF. The height of this projected area is equal to $\partial p_{CBL}/\partial\theta_{ep}$, while the width of the area is equal to $\partial\theta_{ep}^*/\partial p \times \Delta p$. The undilute cloud divergence δ_{cu} will equal this projected area, normalized by the Δp of the pressure interval, and divided by the time scale at which the available boundary layer mass is removed by convection,

$$\delta_{cu}(\theta_{ep}^*) = \frac{\partial p_{CBL}}{\partial\theta_{ep}}\frac{\partial\theta_{ep}^*}{\partial p}\left(\frac{1}{\tau_{rem}}\right). \tag{15}$$

We will assume that the convective removal time scale τ_{rem} is independent of θ_{ep} and is equal to 2 days. The implementation of this assumption in a Monte Carlo model gave rise to boundary layer θ_{ep} PDFs that were in good agreement with those observed (Folkins and Braun 2003).

Figure 11 compares the undilute cloud-mass divergence profile δ_{cu} predicted by (15) with the mass divergence profile δ_c obtained from the one-dimensional diagnostic model. The two profiles have a common shape. They both show a deep outflow layer extending from roughly 10 to 16 km, an interval between 6 and 10 km where the cloud-mass divergence is weak, and enhanced cloud-mass divergence below 6 km.

In the undilute ascent model, cloud outflow is enhanced where there are strong vertical gradients in θ_{ep}^*. Cloud divergence is weak between 5 and 10 km because of the pseudoadiabatic temperature stratification of this interval.

Above 10 km, the θ_{ep}^* density of states ($\partial\theta_{ep}^*/\partial p$) increases with height, while the available boundary layer mass ($\partial p_{CBL}/\partial\theta_{ep}$) decreases with height. The undilute cloud-mass divergence δ_{cu} is, therefore, largest at an intermediate altitude (~14 km) where their product is maximized.

In Fig. 11, the cloud-mass divergence profile of the diagnostic model (δ_c) is shifted downward from the undilute cloud-mass divergence profile (δ_{cu}) by about 1.5 km ($\Delta\theta$ ~7 K). This downward shift is presumably a result of the entrainment of lower θ_{ep} air during ascent. A difference in potential temperature of 7 K corresponds, at 300 mb, to a temperature difference of 5 K. This is comparable with the positive temperature buoyancies associated with undilute pseudoadiabatic ascent from the surface (e.g., Zipser 2003). A reduction of 7 K in θ is therefore roughly consistent with the amount of entrainment that would be required to generate the very weak cloud updraft speeds associated with deep convection over the tropical oceans (Jorgensen and LeMone 1989; Lucas et al. 1994).

8. What controls evaporative moistening in the pseudoadiabatic layer?

Figure 9 shows that evaporative moistening is the dominant source of water vapor to most of the tropical troposphere. On small scales, the rate of evaporative

moistening will be controlled by the surface area of falling precipitation, and the relative humidity of the air in which it is falling. There is, however, a large-scale constraint on the magnitude of evaporative moistening which arises from the role that this process plays in the vertical mass flux budget of the clear-sky atmosphere.

The temperature stratification within the pseudoadiabatic layer favors a weak cloud-mass divergence ($\delta_c \approx 0$), so that the cloud-mass flux ω_c is roughly independent of height (see Fig. 4). As discussed earlier, the sum of the tropical mean vertical mass fluxes associated with clear-sky radiative cooling, precipitation-induced evaporative cooling, and all diabatic processes inside clouds must approximately sum to zero. The rate of precipitation-induced evaporation within the pseudoadiabatic layer must therefore vary in such a way that

$$\omega_r + \omega_e = -\omega_c \approx \text{constant}. \tag{16}$$

The rate of precipitation-induced evaporation determines ω_e through (4). It also has a significant influence on ω_r, because of the sensitivity of the tropical mean clear-sky radiative rate Q_r to the mean relative humidity profile. It is therefore most appropriate to think of (16) as a self-consistency constraint on e within the pseudoadiabatic layer. One method of determining the extent to which this constraint is obeyed in the current climate is to compare the relative humidity profile obtained from (16) with observed mean profiles. This comparison is shown in Fig. 8. Within the pseudoadiabatic layer, the relative humidity profile obtained from (16), labeled $\delta_c = 0$, successfully reproduces the variation of the mean relative humidity with height.

To solve for ω_e from (16), ω_c was fixed at its value at 8 km obtained from the diagnostic model, and ω_r was obtained from the tropical mean profile shown in Fig. 4. Then, e was obtained from ω_e using (4). The water vapor mixing ratio gradient $\partial r/\partial p$ was then determined from (2) using the assumption that $d = 0$ (consistent with the assumption $\delta_c = 0$). The r profile was obtained by fixing r at its observed 8-km tropical mean value. The $\delta_c = 0$ relative humidity profile shown in Fig. 8 was therefore forced to reproduce the observed tropical mean relative humidity at 8 km. However, the degree to which this profile is consistent with the observed mean relative humidity above and below 8 km gives an indication of the vertical extent over which (16) is a useful constraint on humidity levels in the midtroposphere.

9. Conclusions

In the Tropics, deep cumulonimbus clouds coexist with a population of ubiquitous shallow cumuli. The outflow from the cumulonimbus clouds is preferentially distributed within a deep outflow layer (~10–17 km), while the outflow from the shallow cumuli is distributed within a shallow outflow layer (~2–5 km). Each of the two cloud types imposes a mass flux divergence on the tropical atmosphere, which by conservation of mass, must be balanced by a mass flux convergence in the clear-sky atmosphere. The tropical mean diagnostic model used in this paper shows that, while the mass flux divergence of cumulonimbus clouds is balanced by a radiative mass convergence in clear-sky regions, the mass flux divergence of shallow cumuli is balanced by a mass flux convergence associated with evaporatively driven downdrafts (considered in this paper to be a clear-sky process when it moistens the background clear-sky atmosphere).

While deep and shallow convection can be differentiated on the grounds that their mass flux divergences are balanced by distinct physical processes, they are strongly coupled. Shallow convection is forced by deep convection because the downdrafts that initiate shallow convection in the mesoscale and regional environment arise mainly from deep convective precipitation. On the other hand, shallow convection favors the development of deep (and more nearly undilute) convection by diminishing the contrast between the pseudoequivalent potential temperature θ_{ep} of deep convective updrafts and their environment. Although the relationship between deep and shallow convection is complicated, it seems likely that future increases in the height of the melting level (e.g., Diaz and Graham 1996) due to increased tropical sea surface temperatures will increase the height interval over which evaporative cooling dominates the tropical mean dry static energy budget and increase the relative importance of shallow convection in the Hadley circulation.

Within the shallow outflow layer, the tropical mean static stability is proportional to the tropical mean clear-sky heating rate. As a result, the tropical mean clear-sky radiative mass flux is independent of height and the radiative mass flux divergence is near zero ($\delta_r \approx 0$). The argument that the mass divergence from shallow cumuli is offset by a mass divergence from precipitation-induced evaporation ($\delta_c + \delta_e \approx 0$) is therefore a direct consequence of the vertical variation of the tropical mean temperature and radiative cooling profiles in the shallow outflow layer.

The undilute ascent model was used to generate a deep convective divergence profile from the probability distribution function of θ_{ep} in the boundary layer. The peak of this undilute deep convective divergence profile is near 14 km, while the peak of the deep convective divergence profile diagnosed from observed temperature and relative humidity profiles is near 12.5 km. This offset in height confirms that most deep convective updrafts do entrain lower θ_{ep} air during ascent. The magnitude of this offset is roughly consistent with the amount of entrainment that would be required to reduce undilute updraft velocities to their observed values. Undilute ascent is only required for those few air parcels that reach the tropical tropopause.

Although the concept of undilute ascent is of limited use for predicting updraft velocities in the Tropics, it is

useful for understanding the overall shape of the tropical mean cloud mass flux divergence profile. In particular, the undilute ascent model demonstrates that the inhibition of convective outflow between 5 and 10 km can be attributed to the pseudoadiabatic temperature stratification of this interval.

The dominant source of water vapor to the midtropical troposphere is evaporative moistening. Below 12 km, this moistening gives rise to a downward mass flux which becomes increasingly comparable with the downward mass flux from radiative cooling. This coupling of the water vapor and mass budgets gives rise to a constraint on the strength of evaporative moistening. Within the pseudoadiabatic layer (5–10 km), the weakness of the cloud-mass divergence implies that the cloud-mass flux ω_c is roughly independent of height. This, in turn, forces the sum of the mass fluxes from radiative and evaporative cooling to be approximately independent of height ($\omega_r + \omega_e \approx$ constant). The application of this constraint gives rise to a relative humidity profile that is in good agreement with observations between 5 and 10 km. More generally, the vertical variation of evaporative moistening between 5 and 10 km should be realistic in any model of the Tropics in which (i) the strength of the deep convective component of the Hadley circulation is realistic (i.e., ω_c is realistic), (ii) the cloud mass flux divergence between 5 and 10 km is weak, and (iii) the tropical mean clear-sky radiative mass flux has the correct dependence on height between 5 and 10 km.

Between 12 and 15 km, the observed increase in tropical mean relative humidity with height can be reproduced by the assumption of a first-order balance between detrainment moistening and subsidence drying. However, there are not enough in situ measurements of water vapor in this height interval to generate a geographically representative relative humidity climatology. The inference that evaporative moistening does not play a significant role in the water vapor budget between 12 and 15 km should therefore be regarded as tentative.

Acknowledgments. The NOAA/NCDC high-resolution radiosonde data were provided by the SPARC Data Center from their Web site (available at http://www.sparc.sunysb.edu/html/hres.html). Reynolds SST data were provided by the NOAA–CIRES Climate Diagnostics Center, Boulder, Colorado, from their Web site (available at http://www.cdc.noaa.gov/). We thank the Natural Sciences and Engineering Research Council of Canada, the Modeling of Global Chemistry for Climate (GCC) project, the Canadian Foundation for Climate and Atmospheric Sciences (CFCAS), and the Atmospheric Chemistry Experiment (ACE) for their support. The GEOS-CHEM model is managed by the Atmospheric Modeling Group at Harvard University with support from the NASA Atmospheric Chemistry Modeling and Analysis Program. This paper was substantially modified by the comments of three reviewers. Their input is gratefully acknowledged.

REFERENCES

Ackerman, T. P., K.-N. Liou, F. P. J. Valero, and L. Pfister, 1988: Heating rates in tropical anvils. *J. Atmos. Sci.,* **45,** 1606–1623.

Betts, A. K., 1973: A composite mesoscale cumulonimbus budget. *J. Atmos. Sci.,* **30,** 597–610.

Dessler, A. E., and S. C. Sherwood, 2000: Simulations of tropical upper tropospheric humidity. *J. Geophys. Res.,* **105,** 20 155–20 163.

Diaz, H. F., and N. Graham, 1996: Recent changes in tropical freezing heights and the role of sea surface temperature. *Nature,* **383,** 152–155.

Folkins, I., 2002: Origin of lapse rate changes in the upper tropical troposphere. *J. Atmos. Sci.,* **59,** 992–1005.

——, and C. Braun, 2003: Tropical rainfall and boundary layer moist entropy. *J. Climate,* **16,** 1807–1820.

——, ——, A. M. Thompson, and J. C. Witte, 2002a: Tropical ozone as an indicator of deep convection. *J. Geophys. Res.,* **107**, 4184, doi:10.1029/2001JD001178.

——, E. J. Hintsa, K. K. Kelly, and E. M. Weinstock, 2002b: A simple explanation for the relative humidity increase between 11 and 15 km in the Tropics. *J. Geophys. Res.,* **107**, 4736, doi:10.1029/2002JD002185.

Fu, Q., and K. N. Liou, 1992: On the correlated k-distribution method for radiative transfer in nonhomogeneous atmospheres. *J. Atmos. Sci.,* **49,** 2139–2156.

Holton, J. R., 1992: *An Introduction to Dynamic Meteorology.* Academic Press, 511 pp.

Houze, R. A., 1997: Stratiform precipitation in regions of convection: A meteorological paradox? *Bull. Amer. Meteor. Soc.,* **78,** 2179–2196.

Johnson, R. H., P. E. Ciesielski, and K. A. Hart, 1996: Tropical inversions near the 0°C level. *J. Atmos. Sci.,* **53,** 1838–1855.

——, and Coauthors, 1999: Trimodal characteristics of tropical convection. *J. Atmos. Sci.,* **56,** 2397–2418.

Jorgensen, D. P., and M. A. LeMone, 1989: Vertical velocity characteristics of oceanic convection. *J. Atmos. Sci.,* **46,** 621–640.

LeMone, M. A., E. J. Zipser, and S. B. Trier, 1998: The role of environmental shear and CAPE in determining the structure and evolution of mesoscale convective systems during TOGA COARE. *J. Atmos. Sci.,* **55,** 3493–3518.

Lucas, C., E. J. Zipser, and M. A. LeMone, 1994: Vertical velocity in oceanic convection off tropical Australia. *J. Atmos. Sci.,* **51,** 3183–3193.

Mapes, B. E., 1995: Diabatic divergence profiles in western Pacific mesoscale convective systems. *J. Atmos. Sci.,* **52,** 1807–1828.

——, 2000: Convective inhibition, subgrid-scale triggering energy, and stratiform instability in a simple tropical wave model. *J. Atmos. Sci.,* **57,** 1515–1535.

——, 2001: Water's two height scales: The moist adiabat and the radiative troposphere. *Quart. J. Roy. Meteor. Soc.,* **127,** 2353–2366.

——, and R. A. Houze, 1993: An integrated view of the 1987 Australian monsoon and its mesoscale convective systems. II: Vertical structure. *Quart. J. Roy. Meteor. Soc.,* **119,** 733–754.

Martin, R. V., D. J. Jacob, R. M. Yantosca, M. Chin, and P. Ginoux, 2003: Global and regional decreases in tropospheric oxidant from photochemical effects of aerosols. *J. Geophys. Res.,* **108,** 4097, doi:10.1029/2002JD002622.

May, P. T., and D. K. Rajopadhaya, 1996: Wind profiler observations of vertical motion and precipitation microphysics of a tropical squall line. *Mon. Wea. Rev.,* **124,** 621–633.

Pierrehumbert, R. T., 1998: Lateral mixing as a source of subtropical water vapor. *Geophys. Res. Lett.,* **25,** 151–154.

Randall, D. A., Harshvardan, D. A. Dazlich, and T. G. Corsetti, 1989: Interactions among radiation, convection, and large-

scale dynamics in a general circulation model. *J. Atmos. Sci.,* **46,** 1943–1970.

Read, W. G., J. W. Waters, D. L. Wu, E. M. Stone, and Z. Shippony, 2001: UARS Microwave Limb Sounder upper tropospheric humidity measurement: Method and validation. *J. Geophys. Res.,* **106,** 32 207–32 258.

Redelsberger, J. L., D. B. Parsons, and F. Guichard, 2002: Recovery processes and factors limiting cloud-top height following the arrival of a dry intrusion observed during TOGA COARE. *J. Atmos. Sci.,* **59,** 2438–2457.

Reynolds, R. W., N. A. Rayner, T. M. Smith, D. C. Stokes, and W. Wang, 2002: An improved in situ and satellite SST analysis for climate. *J. Climate,* **15,** 1609–1625.

Riehl, H., and J. Simpson, 1979: The heat balance of the equatorial trough zone, revisited. *Contrib. Atmos. Phys.,* **52,** 287–305.

Rossow, W. B., and R. A. Schiffer, 1999: Advances in understanding clouds from ISCCP. *Bull. Amer. Meteor. Soc.,* **80,** 2275–2302.

Thompson, A. M., 2001: Organization of tropical convection in low vertical wind shears: The role of water vapor. *J. Atmos. Sci.,* **58,** 529–545.

——, and Coauthors, 2003: Southern Hemisphere Additional Ozonesondes (SHADOZ) 1998–2000 tropical ozone climatology. 1. Comparison with Total Ozone Mapping Spectrometer (TOMS) and ground-based measurements. *J. Geophys. Res.,* **108,** 8238, doi:10.1029/2001JD000967.

Trenberth, K. E., D. P. Stepaniuk, and J. M. Caron, 2004: The global monsoon as seen through the divergent atmospheric circulation. *J. Climate,* **17,** 3969–3993.

Yanai, M., S. Esbensen, and J. Chu, 1973: Determination of bulk properties of tropical cloud clusters from large-scale heat and moisture budgets. *J. Atmos. Sci.,* **30,** 611–627.

Zhang, C., and M. McGauley, 2004: Shallow meridional circulation in the tropical eastern Pacific. *J. Atmos. Sci.,* **61,** 133–139.

Zipser, E. J., 2003: Some views on "hot towers" after 50 years of tropical field programs and two years of TRMM data. *Cloud Systems, Hurricanes, and the Tropical Rainfall Measuring Mission* (*TRMM*)*, Meteor. Monogr.,* No. 51, Amer. Meteor. Soc., 49–58.